Study of zone-folding effects on phonons in alternating monolayers of GaAs-AlAs

A. S. Barker, Jr., J. L. Merz, and A. C. Gossard
Bell Laboratories, Murray Hill, New Jersey 07974
(Received 12 July 1977)

Samples prepared with one, two, and four atomic layers of GaAs alternating with similar layers of AlAs have been studied by Raman and infrared spectroscopy. The new lattice periodicity along the growth direction is predicted to cause gaps in the phonon spectra and certain new zero-wave-vector modes. New modes are observed in the spectra in the range 150–380 cm^{-1} which are ascribed to the layering effects. Comparisons with random alloy samples and with detailed model calculations of mode frequencies and strengths show that layering is present in the samples, and allow a semiquantitative determination of the degree of order of the structures.

I. INTRODUCTION

Over the past ten years, the technique of molecular-beam epitaxial growth has been developed as a method of creating extremely thin crystalline layers.[1] Considerable work has gone into the development of methods to grow alternating ~100-Å layers of, for example, GaAs and AlAs, repeated a sufficient number of times to create crystals of micron dimensions. The superlattice periodicity of such crystals is much longer than the atom spacing and can be controlled to produce specific effects. In some of the earlier work the motivation was to create negative-resistance regions due to band-bending effects and the gaps which arise from the new lattice periodicity.[2] Optical spectroscopy has been used to detect transitions from sharp quantum states arising from electrons or holes confined by such synthetically created periodic structures.[3,4] Transitions have been detected for layer thicknesses in the range 40–400 Å. Recently, still thinner GaAs and AlAs layers, of thicknesses as small as 2.8 Å, have been grown. Transmission-electron-microscopy results have confirmed the existence of layers as thin as one or two monolayers in some crystals,[5] although these studies also gave evidence for some disorder in the structures.

It has long been realized that lattice vibrations provide a probe of crystal structure with a scale of 2 to 4 Å. This short-range scale arises from the strong dependence of the vibration on nearest-neighbor bonds. In contrast to the optical spectroscopy of electron wave functions which can deform around an impurity or misplaced ion with little change in energy, the lattice vibration energy can be very sensitive to such defects. In the present study, the lattice vibrations of layered structures of GaAs-AlAs are examined by infrared and Raman spectroscopy.[6] Layers ranging from monolayer to tetralayer thickness producing lattice periodicities of 5.7 to 22.6 Å are measured. Additional random alloy samples of $Al_xGa_{1-x}As$ are included in the study so that lattice-vibration effects connected with true layering and the concomitant folding of the Brillouin zone may be distinguished from effects associated with disorder. In the layered crystal, the existence of a new long period causes the primitive unit cell to be enlarged over that of either GaAs or AlAs. This enlargement creates many extra phonon branches. The extra or new lattice vibrations may be understood on the basis of zone folding, where the first Brillouin zone of the pure crystal (e.g., GaAs) is folded in along one direction in k space (corresponding to the growth direction) to create new zone-center modes.

In contrast to the crystals studied here, some solids occur naturally in so-called polytype systems which exhibit layering along one direction.[7] Vibrations corresponding to the zone-folding effect have been detected in these solids, but were found to be a very small perturbation of the phonon branches of the unlayered structure.[8,9] This is a small perturbation in polytype systems because the nearest-neighbor species, bond lengths, and bond angles to any atom are always the same; the polytype formation is caused by various possible stacking arrangements. The GaAs-AlAs alternating monolayers discussed here, on the other hand, are the first realization of single-crystal synthetic layered material. In these crystals some As ions see four Ga, some see four Al and some see two Ga and two Al as nearest neighbors. These configurations therefore represent large perturbations and the corresponding gaps which open in the phonon dispersion curves are large and must be calculated in detail. In this situation, we find it necessary to use an explicit model to calculate the frequencies and the mode strengths, both for Raman scattering and infrared absorption. These model results, when compared with the experi-

ments, allow conclusions to be drawn on the layering and, equally as important, on the degree of perfection of the layers. To illustrate the various effects we find it convenient to first develop the lattice-vibration model in Sec. II. In Sec. III the phonon symmetry is discussed in terms of symmetry operations which occur in layered structures and results are obtained which are independent of any model. Sections IV–VI present the details of sample preparation and the methods of measuring the Raman and infrared spectra and reducing the data. Discussions of the results are given in these sections and Sec. VII lists the conclusions.

II. LATTICE VIBRATION MODEL

A. Frequencies and eigenvectors

Figure 1 shows the model used to calculate the lattice-vibration frequencies, as well as the infrared and Raman strengths. It is a linear chain model.[10] All of the crystals studied were grown on an (001) oriented substrate of GaAs and showed x-ray diffraction characteristic of this growth, i.e., new spots due to the new periodicity along the z axis, but retaining the symmetry operations which make the x and y axes equivalent. We assume that these properties are sufficient to allow the complete separation of longitudinal and transverse vibrations for phonons with the wave vector parallel to the z axis. For the ideal crystal, group theory shows that for the wave vector parallel to z, the vibration problem is naturally diagonal with transverse vibrations belonging to one representation and longitudinal vibrations to another.[11] Using this fact we see that the use of one-dimensional models is an exact representation of the vibrations for $\vec{k}=(0,0,k_z)$ as long as appropriate force constants are used.

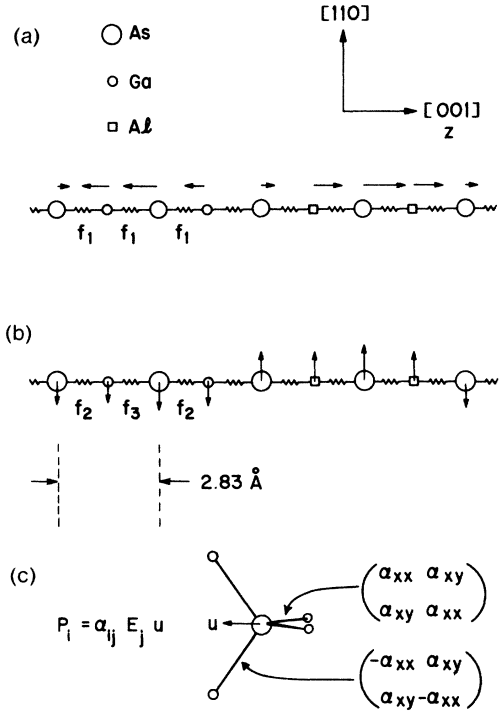

FIG. 1. Linear-chain models for pure and layered crystals. (a) Model for longitudinal vibrations using one force constant f_1 and displacements along [001]. (b) Model for transverse vibrations with two shearing force constants and displacements along [110]. The eigenvectors illustrated are for a (2,2) layered crystal and each lies just above the small gap at $k=0$ shown in Fig. 3. (c) Definition of polarizability matrix for bonds surrounding an As ion which moves with displacement u with respect to its neighbors.

In Fig. 1(a) we show the model for longitudinal vibrations with force constants f_1, which we take to have the same value throughout the lattice. Figure 1(b) shows the model for transverse vibrations with force constants f_2 and f_3. To explain the very-low-lying transverse-acoustical phonon branch in GaAs,[12] and in other related materials such as Ge and Si, f_3 must be extremely weak compared with the other force constants. An examination of the real three-dimensional crystal shows that the small value of f_3 is associated with the pure bending force constant which occurs for every second plane of bonds when we pick the wave vector along [001] and the vibration direction along [110]. Table I gives the values of the force constants actually used, and some other parameters connected with the model. Note that we include no Coulomb or long-range polarization effects so that the TO-LO splitting is determined only by the force constants, and is independent of the charges used. The charges are introduced to obtain infrared mode strengths and are chosen to agree with experimental mode strengths for the pure crystals. The nearest-neighbor force constants have been chosen to fit known frequencies of pure GaAs; with three force constants we can fit three frequencies, as shown by the solid arrows in Fig. 2(a).

We regard the replacement of Ga by Al as a mass change only. Using the masses appropriate for AlAs with our chosen force constants results in the phonon dispersion curves shown in Fig. 2(b). This approach of using the same force constants for GaAs and AlAs does a reasonable job of fitting the known zone-center[13] and zone-boundary (X point)[14] frequencies in AlAs which are shown in the figure by the arrows. From Fig. 2 we note that our three-force-constant model is somewhat in error in predicting some zone-boundary frequencies in GaAs and AlAs.[15] This error can be

TABLE I. Force constants, charges, and mode strengths for model calculations.

	GaAs	AlAs
Charges	$Z^+ = 2.16\|e\|$	$2.20\|e\|$
	$Z^- = -2.16\|e\|$	$-2.20\|e\|$
Force constants	longitudinal $f_1 = 0.9 \times 10^5$ dyn/cm	
	transverse $\begin{cases} f_2 = 1.42 \times 10^5 \\ f_3 = 0.13 \times 10^5 \end{cases}$	
Cell volume per ion pair	45.3 Å^3	45.3 Å^3
ϵ_∞	11.1	8.2
Infrared mode[a] strength S	1.93	2.0
Mode strength[b]	$S = \frac{2}{\pi}\int_0^\infty \frac{\mathrm{Im}(\epsilon)\,d\omega}{\omega} = \frac{2c}{\pi}\int_0^\infty \frac{n\alpha\,d\omega}{\omega^2}$	
Raman[c] polarizability	$\alpha_{xx} = 6.0$	$\alpha_{xx} = 1.2$
	$\alpha_{xy} = 1.0$	$\alpha_{xy} = 0.3$

[a] These are the best measured values.

[b] ϵ is the complex dielectric constant, $n + ik$ the complex index and α the power absorption coefficient. $\alpha = 2k\omega/c$ where c is the velocity of light in vacuum.

[c] These coefficients refer to the crystal x, y axes and the pair of bonds and unit ion amplitude shown in Fig. 1(c).

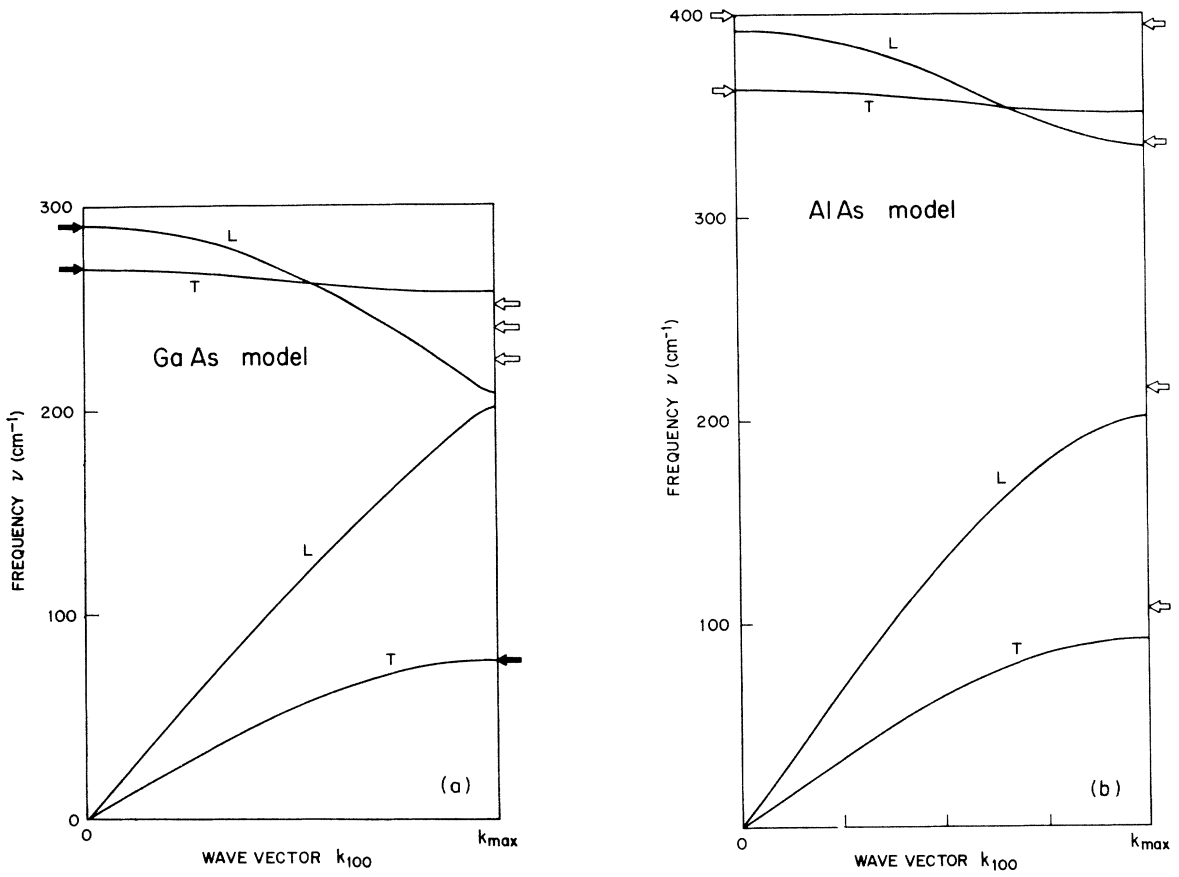

FIG. 2. (a) Phonon dispersion of longitudinal and transverse branches of pure GaAs obtained from model of Fig. 1 and parameters of Table I. The force constants were adjusted to give the three frequencies shown by solid arrows. The three open arrows show frequencies at three other locations known from neutron scattering. (b) Phonon dispersion for AlAs using the force constants which fit GaAs. A reasonable fit is obtained to the known frequencies of AlAs (shown by open arrows) if we relabel the assignments of Ref. 14 T, L, L, T in order of ascending frequency at the zone boundary. Recent work on phonon sidebands supports this assignment.

considerably reduced by choosing appropriate second-neighbor Ga-Ga and As-As force constants. Al-Al force constants would be necessary in AlAs and in any layered crystals.[16] However, aside from test calculations, we have not included these additional force constants in the model which we present here because of the additional complexity which results, because the Al-Al force constant is unknown and because the frequency error has the right sign and magnitude for the shift we expect in the lower L branch when GaAs and AlAs are combined.[15]

Figure 3 shows the phonon dispersion curves calculated from our model for a (1,1) layered crystal and for a (2,2) layered crystal. We use the notation (n,m) to mean n layers (each 2.83 Å thick) of GaAs followed by m layers of AlAs (each 2.83 Å thick) and then the sequence is repeated. For model calculations, n and m are integers. For real samples, noninteger n and m are possible as discussed below. The lengthened period in the (1,1) and (2,2) crystals results in zone folding and the appearance of gaps in the previously

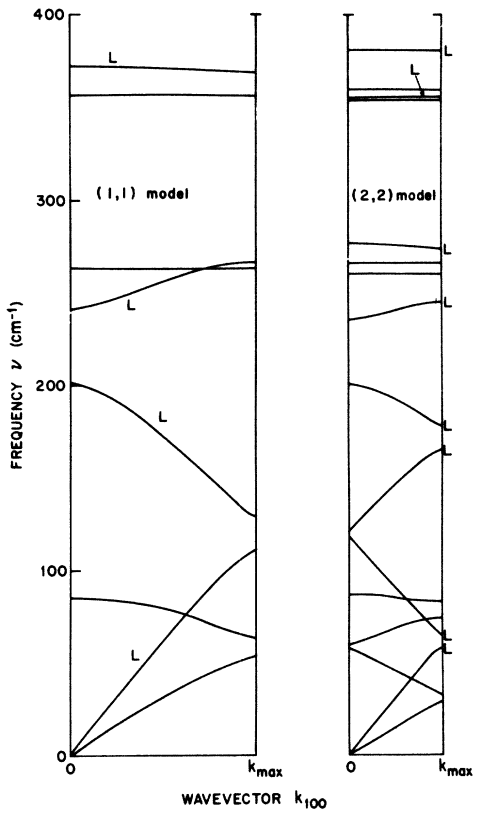

FIG. 3. Model results for (1,1) and (2,2) layered crystals. Note the many new $k=0$ modes and the gaps at the zone center and zone edge. Branches containing longitudinal modes are labeled L. Unlabeled branches contain transverse modes.

smooth phonon branches. Note that the replacement of a Ga atom by an Al atom is a large perturbation. In the (1,1) or monolayer-monolayer case this causes two distinct and well-separated optic branches (Fig. 3). In the (2,2) or bilayer-bilayer case there are also two groups of optic modes with a large separation between them. An examination of individual eigenvectors shows considerable localization in the highest branches with most of the vibrational amplitude on the Al atoms.

B. Mode strengths

Infrared mode strengths are calculated for the various models of the pure and layered crystals described above by assigning the charges shown in Table I. The results are presented in terms of the dimensionless integrated mode strength S_j,[17] which is related to the complex dielectric constant and the complex index of refraction as shown in Table I.

Figure 3 shows that there can be many new zone-center modes. However, some of these modes have a strength which is rigorously zero. Many of the remaining modes have very weak strengths. The reason for this is illustrated in Figs. 1(a) and 1(b) for the (2,2) case. Here we show the eigenvector for a zone-center mode caused by the new fourfold lattice periodicity. Note that the displacement pattern arises from a mode which in the pure crystal was halfway to the zone boundary. In the pure crystal, the positive and negative displacements shown in the figure exactly cancel so that there is no net dipole moment. For the layered crystal, the displacement pattern is perturbed by the lighter mass of the Al so that the perfect cancellation of dipole moment is partially destroyed. The mode in Fig. 1(b) has a strength $S=0.0039$ which is 500 times weaker than the zone-center mode in pure GaAs.

Table II lists the mode strengths for transverse vibrations of the type shown in Fig. 1 for the two pure crystals and three cases of layered crystals. Similar linear-chain calculations for a (5,5) crystal have been reported by Tsu and Jha.[18] They do not use the very asymmetric forces (f_2 and f_3) which we believe are necessary to describe the transverse vibrations, nor do they carry out an analysis of longitudinal vibrations and Raman strengths. Their results for the infrared mode strengths are similar to our results for a (5,5) crystal and they point out some details of the polariton region at the small wave vector.

Because of the complexity of the Raman tensor for layered crystals, we restrict ourselves to evaluating the components which can be detected in our experimental setup. As explained below

TABLE II. Model calculations of zone-center mode strengths and frequencies.

Transverse modes—infrared strengths			
GaAs		AlAs	
$\bar{\nu}_j$(cm^{-1})	S_j	$\bar{\nu}_j$(cm^{-1})	S_j
269.0	1.93	363.0	2.0
Monolayer (1,1)		Bilayer (2,2)	
85.2	0.008 7	57.5	0.0
262.8	0.82	59.0	0.0039
357.8	1.13	86.2	0.0
Tetralayer (4,4)		260.4	0.0
30.9	0.000 01	266.2	0.90
31.4	0.000 91	354.6	0.0
57.5	0.000 09	360.5	1.06
59.0	0.0		
74.5	0.0		
79.4	0.000 99		
88.6	0.0		
258.6	0.0		
261.6	0.047		
265.2	0.0		
267.9	0.88		
352.7	0.0		
355.8	0.061		
359.4	0.0		
362.2	0.97		

only modes with both wave vector and displacements approximately parallel to the [001] direction can be detected [i.e., longitudinal vibrations, such as the mode shown in Fig. 1(a)]. Polarizers can be used to detect xx and xy scattering for this geometry.

In Fig. 1(c) we sketch the elements we include in the model. The Stokes polarization P_i (where the index i refers to the crystalline x or y axis) is proportional to a polarizability coefficient α times the laser field E times a characteristic [001]-directed phonon amplitude u. We consider each bond shown by the straight lines in Fig. 1(c) to carry a bond charge which contributes to the total crystal polarizability. Under the action of the displacement u shown in the figure, the bond charge is rotated and also compressed or extended. The fundamental bond polarizabilities $\alpha_{\parallel}$ and $\alpha_{\perp}$ (parallel and perpendicular to the bond) are elements of the model, as well as the change in $\alpha_{\parallel}$ with respect to bond length. We take the change in $\alpha_{\perp}$ with bond length to be negligibly small.

Evaluating all these parameters using the geometry of the tetrahedron and the transformation of coordinates from the plane of the bonds to the crystalline x and y axes which are 45 deg away, we obtain a 2×2 matrix of coefficients as shown in the figure. An estimate of the fundamental bond polarizabilities suggests that α_{xx} and α_{xy} are approximately equal. The two bonds to the left of the atom which is moving with displacement u in the figure produce coefficients of the same magnitudes, however α_{xx} is reversed in sign. By symmetry $\alpha_{xx}=\alpha_{yy}$; therefore there are two independent coefficients α_{xx} and α_{xy} for a Ga-As bond and two for an Al-As bond. These four polarizabilities are now regarded as fundamental parameters. Since we make no absolute cross-section measurements we choose $\alpha_{xy}(\mathrm{GaAs})=1.0$ and have three parameters to determine.

Table I shows the values finally adopted based on the assumptions above and on fitting the three strongest features in the (4,4) sample. In parallel with our discussion of force constants we assume here that the fundamental polarizability coefficients retain their pure crystal values, i.e., an AlAs bond in the layered crystal has the same polarizability coefficients as it would have in pure AlAs. The polarizabilities are combined with the bond extension or compression u of each bond obtained from the normalized eigenvector of the model, and are then added together for the entire crystal and squared. The result is then multiplied by the thermal (Stokes) factor to yield a relative Raman-scattering strength R_{xx} and R_{xy} for that particular mode.[19]

An important result of the model calculations and fits is the difference in infrared strengths and Raman polarizabilities. The Ga and Al effective charges are almost equal, causing the new zone-center modes to be extremely weak in infrared absorption. The polarizabilities however are quite different for Ga and Al bonds. This causes enhanced Raman "visibility" of some of the new modes caused by layering. Table II and succeeding tables and figures show the resulting Raman strengths.

Eigenvectors and mode strengths have also been calculated for many disordered chain models in an effort to understand the spectra observed for several of the samples. One of the most striking effects occurs in (1,1) crystals.

As illustrated by Table III and Fig. 3, we find that the highest frequency of the longitudinal-acoustical branch becomes a zone-center mode at 201.4 cm^{-1} (in our model) for many sequences of layering. Only for sequences with $n=m$ odd, however, are the phases of the motion correct to cause nonzero Raman strength. This same phonon branch is often invoked in analyzing weak modes in disordered crystals. Such an assignment was used by Tsu *et al.*[20] to explain their disorder-activated-longitudinal-acoustical (DALA) mode at 198 cm^{-1}. It is clear, therefore, that study of the mode structure near 200 cm^{-1} can yield valuable information on the perfection of the layered crys-

TABLE III. Model calculations of zone center mode strengths and frequencies.

Longitudinal modes—Raman strengths					
GaAs			AlAs		
$\bar{\nu}_j$(cm^{-1})	R_{xx}	R_{xy}	$\bar{\nu}_j$(cm^{-1})	R_{xx}	R_{xy}
289.0	0.0	6.7	391.4	0.0	0.72
Monolayer (1,1)			Bilayer (2,2)		
201.4	32.7	0.0	118.4	24.5	0.0
241.3	0.0	2.41	120.8	0.0	0.11
372.1	0.0	1.18	201.4	0.0	0.0
Tetralayer (4,4)			236.4	3.02	0.0
60.9	20.0	0.0	277.3	0.0	2.86
61.9	0.0	0.022	356.1	1.03	0.0
118.4	0.0	0.002	381.8	0.0	0.68
120.7	0.42	0.0			
168.6	3.22	0.0			
172.7	0.0	0.029			
201.4	0.0	0.0			
227.8	1.41	0.0			
253.3	0.0	0.19			
272.6	0.26	0.0			
285.5	0.0	2.90			
344.4	0.19	0.0			
361.6	0.0	0.11			
377.4	0.22	0.0			
387.8	0.0	0.44			

tals.

The following set of model calculations was made to this end. Consider cation occupancy of sites along the chain. Using $P_i = 1$ for occupancy of the ith site by a Ga ion and $P_i = 0$ for occupancy by Al, a perfect (1,1) sample has the occupancy vector

$$\vec{P}(\text{monolayer-monolayer}) = (1,0,1,0,1,0,\ldots).$$

Consider disorder in the form of a single nearest cation pair interchange

$$P(\text{disordered monolayer-monolayer}) = (1,0,0,1,1,0,1,0,\ldots).$$

Eigenvectors, frequencies, and mode strengths have been calculated for a number of such pair interchanges in an otherwise perfect (1,1) chain 48 atoms long with periodic boundary condition. The general result is that as a higher percentage of sites is introduced containing the "wrong ion," the 201-cm^{-1} mode decreases in Raman strength and a band of modes ranging from about 170 to 200 cm^{-1} acquire some Raman activity in both R_{xx} and R_{xy}.

Figure 4 shows the results of these calculations for the Raman strength of modes near 200 cm^{-1}. We conclude by noting again that for the pure crystals and for ordered layered crystals the chain model is in a certain sense exact. If in the model we obtain a displacement u for a Ga ion (say), we are to understand this as the amplitude of all the Ga ions in a plane normal to the z axis. The force constants are therefore interplanar force constants per ion. The model becomes approximate when we include disorder (which is a truly three-dimensional effect) by disordering the one-dimensional model. Previous work has shown that this approximation is useful and has applicability to this type of problem.[21]

III. PHONON SYMMETRY

GaAs is a face-centered-cubic lattice with T_d symmetry ($\bar{4}3m$ in the international notation[22]). For alternating layers grown on (001) planes, this symmetry is reduced to the point group D_{2d} ($\bar{4}2m$). Consider light at normal incidence to the layers, as shown in Fig. 5; this is the geometry used for both Raman and infrared experiments. The incident, scattered, and transmitted wave vectors are given by $\vec{k}_i$, $\vec{k}_s$, and $\vec{k}_t$, respectively, with elec-

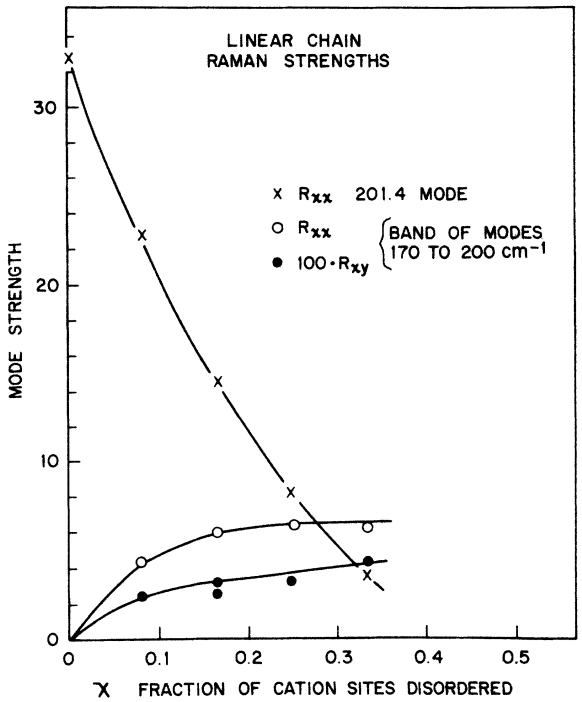

FIG. 4. Calculated Raman mode strengths for ordered and disordered (1,1) chains. The abscissa x describes the fraction of cation Ga ion sites which are occupied by Al ions as described in the text. Calculations were done for $x = 0$, $\frac{1}{12}$, $\frac{1}{6}$, $\frac{1}{4}$, and $\frac{1}{3}$ fractional occupancy by wrong ions; the smooth curves are reasonable interpolations drawn for convenience. $x = 0$ corresponds to a perfect (1,1) layered crystal. The band of modes from 170 to 200 cm^{-1} (circles) corresponds to the DALA mode observed in random alloys (Ref. 20). The (xy) scattering for this band has been scaled up by 100 times to show on the graph.

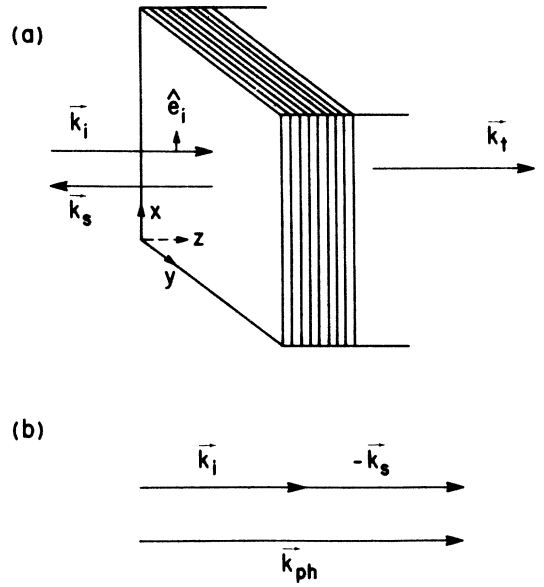

FIG. 5. (a) Geometry for 180° Raman backscattering and infrared absorption. $\vec{k}_i$, $\vec{k}_s$, and $\vec{k}_t$ are the incident, scattered, and transmitted wave vectors, respectively, with electric-field polarization $\hat{e}_i$, etc. The crystal axes of the layered samples (D_{2d} symmetry) are shown. (b) Wave-vector conservation diagram for 180° Raman scattering.

tric-field polarization vectors $\hat{e}_i$, etc. All three wave vectors are parallel to the four-fold rotation axis of the group D_{2d}, chosen to be the z axis.

For Raman scattering, momentum conservation requires

$$\hbar\vec{k}_i = \hbar\vec{k}_s \pm \hbar\vec{k}_{ph}, \tag{1}$$

where $\vec{k}_{ph}$ is the phonon wave vector, and the positive sign holds for Stokes scattering, the case considered here. The vector diagram for 180° backscattering is shown in Fig. 5(b). If the incident beam is polarized in the x direction, as shown in Fig. 5(a), then

$$\hat{e}_i = (1,0,0), \tag{2}$$

$$\hat{e}_s = (1,0,0) \text{ or } (0,1,0). \tag{3}$$

We are, therefore, concerned with the two scattering geometries $z(xx)\bar{z}$ and $z(xy)\bar{z}$.[23] Following the method of Loudon,[24] the irreducible representation of the polarizability tensor for the group D_{2d} must transform as xx (i.e., diagonal representation) or xy, and the phonons observable by Raman scattering for this geometry have symmetry A_1 (Γ_1 in the notation used by Koster *et al.*[25]) for (xx) scattering, and B_2 (Γ_4) for (xy) scattering. Note that the two symmetries are separable for polarizations parallel to the x and y crystallographic axes; for intermediate polarization angles, both symmetry modes are observed. Since the E (Γ_5) representation is not involved, only longitudinal phonons can be detected by the Raman scattering geometry shown in Fig. 5.

The opposite is the case for infrared absorption. The irreducible representation must transform as x or y (for incident and transmitted polarizations in the x or y directions), so the twofold degenerate $E(\Gamma_5)$ representation is infrared active, and only transverse phonons are directly observed. Using the zeros of the dielectric function, however, the frequencies of the longitudinal phonons with polarization along x may be calculated from the data. The infrared absorption measurements are therefore complementary to the Raman-scattering results.

IV. SAMPLE PREPARATION

In order to construct the layered configurations discussed here, the molecular-beam-epitaxy (MBE) technique was used.[1] This involved evaporating beams of gallium, aluminum, and arsenic from separately controlled and shuttered elemental sources. The beams were incident on heated GaAs substrates cut from single-crystal boules and oriented with (001) faces exposed.[1] By sequentially opening the molecular-beam shutters for the amount of time needed to first deposit n monolayers of GaAs and then m monolayers of AlAs, alternating sequences of monolayers were deposited to total thicknesses of several microns. The monolayered compositional structure of such compounds and their interband optical properties have been reported previously.[5] The structures of all samples used in the present work were studied by x-ray diffraction[26] or transmission electron microscopy.[5] Such measurements confirmed that the deposited periodicity, as measured from total deposited film thicknesses, was present in the final samples.

Table IV lists the compositions and thicknesses of the samples studied. For convenience in the remainder of the paper, the sample designation MM refers to (1,1) or alternating monolayer-monolayer samples, BB refers to alternating bilayers, etc.

Generally, the deposited number of monolayers, n and m, were not exactly integral. Such growth has been discussed previously.[5] This factor, together with possible interlayer diffusion and nucleation of second monolayer coverage before completion of an entire first monolayer coverage, set a limit on the order of the structures. Diffraction studies of these effects are in progress[5,26] and some estimates of their magnitude are also attainable from the present phonon spectra. For

TABLE IV. Samples. Values of x_{Al}^{av} are estimated from growth parameters or (in indicated cases) the composition was measured by calibrated Auger spectroscopy. The values (n,m) give the actual numbers of layers in the alternating sequence $(GaAs)_n(AlAs)_m$, as measured by the total thickness of each component divided by the number of shutter cycles.

Sample	x_{Al}^{av}	(n,m)
*MM*1	0.43[a]	(1.22 ± 0.08, 0.98 ± 0.08)
*MM*2	0.51[a]	(1.02 ± 0.06, 0.93 ± 0.09)
*BB*1	0.48	(2.03 ± 0.11, 1.84 ± 0.16)
*BB*2	0.54	(2.04 ± 0.14, 2.37 ± 0.14)
*TT*1	0.46	(4.81 ± 0.28, 4.03 ± 0.28)
*TT*2	0.53	(3.67 ± 0.15, 4.18 ± 0.16)
MB	0.66	(1.15 ± 0.10, 2.48 ± 0.10)[b] (1.08 ± 0.10, 1.90 ± 0.10)
BM	0.38	(2.01 ± 0.10, 1.25 ± 0.10)
*A*29	0.29	
*A*37	0.37	
*A*45	0.45	
*A*48	0.48	
*A*67	0.67	

[a] By Auger spectroscopy.
[b] Measured at opposite edges of sample.

nonintegral depositions, the average period of the compositional structure was found to be $(m+n)$ monolayers, within the experimental accuracy of the diffraction periodicity measurement and the deposition thickness measurements.

For backscattered Raman measurements, the monolayered epitaxial layers were left on the growth substrate. For infrared transmission measurements, however, it was necessary to remove the substrate from the epitaxial layers in order to avoid infrared absorption by the substrate. This was accomplished by grinding away most of the substrate thickness from the substrate side, and then chemically etching away the remainder of the GaAs substrate with a selective etch which is essentially stopped at the substrate-layer interface by the first AlAs monolayer. By covering the area surrounding a selected region with wax, holes of size 2×3 mm could be etched in the substrate, suitable for infrared transmission measurement.

V. RAMAN SCATTERING

A. Experimental method

The Raman scattering from these samples was studied using the 4880-Å line of an argon-ion laser, in a backscattering configuration. Stokes radiation was detected, for which phonons are created and the detected radiation is consequently shifted to lower energy. A Spex $\frac{3}{4}$-m double monochromator was used to disperse the scattered light, which was then detected with an ITT FW130 *Star Tracker* photomultiplier, cooled to −30 °C. For most spectra, the instrumental slitwidth was 300 μm, resulting in an experimental bandwidth of 1.7 Å (6.8 cm^{-1}). Photon-counting techniques were used, and each spectrum was averaged by adding multiple scans (usually three) in a Nicolet signal averager.

In the scattering geometry actually used, the angle of incidence was approximately 45° to facilitate a reasonably large solid angle ($\sim f/1.4$) for collection of the scattered beam. Some "leakage" of scattering from transverse-mode phonons should therefore be observable in the experimental spectra, both for (xx) and (xy) scattering, due to this departure from the strict 180° backscattering that is depicted in the idealized diagram of Fig. 4. However, this effect is minimized by the large refractive index of GaAs, which reduces the scattering angle from 45° to ~10° inside the sample.

The incident laser power was ≤200 mW. The absorption coefficient of GaAs at 2.54 eV (4880 Å) is $\sim 10^5$ cm^{-1}, and varies between 10^5 and 10^4 cm^{-1} for the ternary $Al_xGa_{1-x}As$ alloys and layered structures considered in this work.[27-30] Penetration of the incident beam is therefore ~0.1 to 1.0 μm, so that essentially all of the light is absorbed in the MBE multilayer structure, and a large number of alternating monolayers contribute to the observed scattering. Using published values[31] for the thermal conductivity of $Al_xGa_{1-x}As$ alloys ($0 \leq x \leq 1$), the maximum temperature rise due to laser excitation was estimated to be less than 50 °K.

Scattering of incident laser light into the spectrometer limited the spectral region accessible for study by Raman scattering to frequencies $\nu \geq 150$ cm^{-1} from the incident laser frequency (i.e., $\lambda \geq 4915$ Å). Surface roughness of many of the MBE layers necessitated use of an interference filter with maximum transmission at approximately 4950 Å positioned in front of the spectrometer.[32] In some cases, additional weak lines of the argon discharge were observed in the spectra. These lines occurred at 4906, 4934, 4966, and 4973 Å (which, for many samples, coincides with a strong LO phonon due to Al-As vibrations). An adequate correction for these extraneous lines could often be made by recording spectra with the laser detuned (i.e., discharge on but not lasing), and subtracting the results from the experimental spectra in the signal averager.

B. Raman spectra and LO frequencies

1. Random alloy spectra and disorder activated modes

The Raman scattering spectrum for a typical random alloy is shown in Fig. 6; this sample has an aluminum composition $x_{Al} = 0.45$. The principal

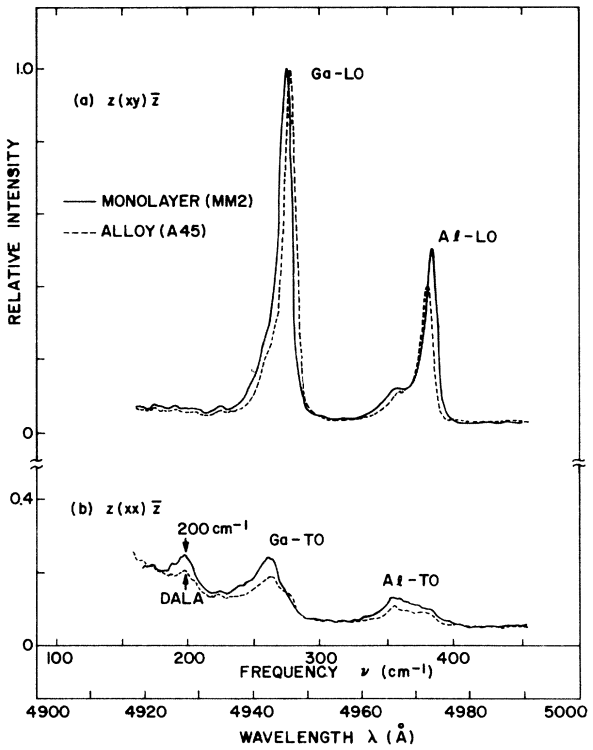

FIG. 6. Raman-scattering spectra for random alloy sample with $x_{Al} = 0.45$, and monolayer sample $MM2$. Traces are given for (a) $z(xy)\bar{z}$ and (b) $z(xx)\bar{z}$ scattering geometries. Other spectral features indicated here are discussed in the text.

GaAs-like and AlAs-like LO phonons are seen at 279 and 381 cm^{-1}, respectively, for (xy) scattering (Γ_4 symmetry). These phonon lines have weak shoulders on the low-energy side, resulting from "leakage" of the TO phonons due to the deviation from true normal incidence described above. The TO phonons are seen more clearly in the trace for (xx) scattering. In addition, the (xx) scattering spectrum has an additional weak line at 198 cm^{-1}, labeled DALA in Fig. 6, which is unanticipated for the usual zone-center Raman scattering. This phonon mode has been observed by Tsu *et al.*[20] in their study of Raman scattering from the $Al_xGa_{1-x}As$ alloys. They attribute it to a disorder activated LA mode resulting from a breakdown of the strict selection rules in the alloy material; the frequency of the DALA mode corresponds closely with the L-point zone-boundary LA phonon measured by neutron scattering.[12]

2. Monolayer spectra

The Raman spectrum from monolayer sample $MM2$ is also shown in Fig. 6. In general, the results are very similar to the random alloy spectrum with a comparable average Al composition. However, the results from the model theory developed in Sec. II predict large differences: the Al-As vibration should be shifted 9 cm^{-1} to lower frequency, and the Ga-As mode 38 cm^{-1}, relative to the frequencies of these phonons determined for the random alloy. This has not been observed experimentally, as is clear from the predicted and observed frequencies listed for layered samples in Table V. The model also predicts a strong mode at 201.4 cm^{-1} (which will be referred to as the 201-cm^{-1} mode in subsequent discussion), observable in (xx) symmetry. This occurs at approximately the same frequency as the DALA mode in the random alloy, and also arises from the zone-boundary LA phonon. However, for the layered sample this mode is not disorder activated, but is instead an allowed zone-center phonon resulting from zone folding due to the increased lattice period. Thus, the 201-cm^{-1} mode in alternating monolayer samples should be stronger than DALA in the random alloys. Table VI lists relative strengths observed for the 201-cm^{-1} mode; a slight increase in strength is actually observed for the monolayer samples.

TABLE V. LO-mode frequencies predicted by the linear chain model, and the frequencies of lines observed in Raman scattering, for monolayer and bilayer samples. In addition, the two weak TO modes observed in this scattering geometry are listed. Modes listed in the last two rows are experimentally inaccessible. The mode type refers to the source mode in the parent GaAs or AlAs crystal.[a]

I. Monolayer ($MM2$) Mode type	Symmetry	Predicted (cm^{-1})	Observed (cm^{-1})
AlAs LO	Γ_4	372.1	385
[AlAs TO]	[Γ_5]	[357.8]	[359]
GaAs LO	Γ_4	241.3	275
[GaAs TO]	[Γ_5]	[262.8]	[261]
LA	Γ_1	201.4	198
II. Bilayer ($BB1$)			
AlAs LO	Γ_4	381.8	391
[AlAs TO]	[Γ_5]	[360.5]	[355]
AlAs LO	Γ_1	356.1	
GaAs LO	Γ_4	277.3	280
[GaAs TO]	[Γ_5]	[266.2]	[259]
GaAs LO	Γ_1	236.4	236(?)
LA	Γ_4	201.4[b]	198
LA	Γ_4	120.8	...
LA	Γ_1	118.4	...

[a] For example, the eigenvectors of AlAs LO are composed predominantly of eigenvectors from the LO branch of pure unlayered AlAs.

[b] This mode has zero Raman strength in the linear-chain model.

TABLE VI. Strength of 201-cm^{-1} mode. The ratio R, defined below, is a measure of the strength of the mode at ~201 cm^{-1}. The uncertainty in R is ~±0.01. R = (201-cm^{-1} mode)$_{xx}$/(GaAs LO)$_{xy}$.

Sample	R
$A45$	0.04
$A48$	(~0.13)[a]
$MM1$	0.12
$MM2$	0.07
$BB1$	0.09[b] / 0.06
$BB2$	0.09
TT	0.08

[a] For this sample, the width of the 201-cm^{-1} mode is approximately twice that of other samples, implying the existence of another (unidentified) spectral feature contributing to its apparent strength.

[b] Strengths measured at two different positions on the sample.

3. Bilayer spectra

The 201-cm^{-1} mode tends to be slightly weaker for bilayer samples than observed for monolayer samples, but stronger than the alloys (Table VI). The model predicts that this mode should again be at the zone center, but should have zero strength. The model also predicts a total of five longitudinal modes in the accessible region of the spectrum (Table V). Of the two new predicted modes with Γ_1 symmetry, the mode at 356 cm^{-1} coincides with the stronger Al-As TO vibration which masks it; the Γ_1 mode at 236 cm^{-1} may be present in the (xx) scattering spectrum, but is too weak to be positively identified.

4. Tetralayer spectra

The Raman spectra for the tetralayer sample $TT1$ is shown in Fig. 7. There are two important features in these spectra. The first is the definite shift in energy of the principal AlAs-like and GaAs-like phonons, compared to samples MM, BB, and alloy samples having $X_{Al} \simeq 0.5$ (see Fig. 8). The second feature is the appearance of many new, partially resolved lines on the low-energy side of the principal modes, as predicted by the model. Both of these effects show clear evidence of order and new zone-center phonons in this sample, as will be discussed below.

5. Monolayer-bilayer and bilayer-monolayer samples

Raman-scattering measurements were also carried out for the MB and BM samples. There is little evidence of layering in these samples, but both have rough surfaces, causing strong scattered laser radiation. In both cases some of the additional modes anticipated by the model nearly coincide in energy with stronger TO phonons.

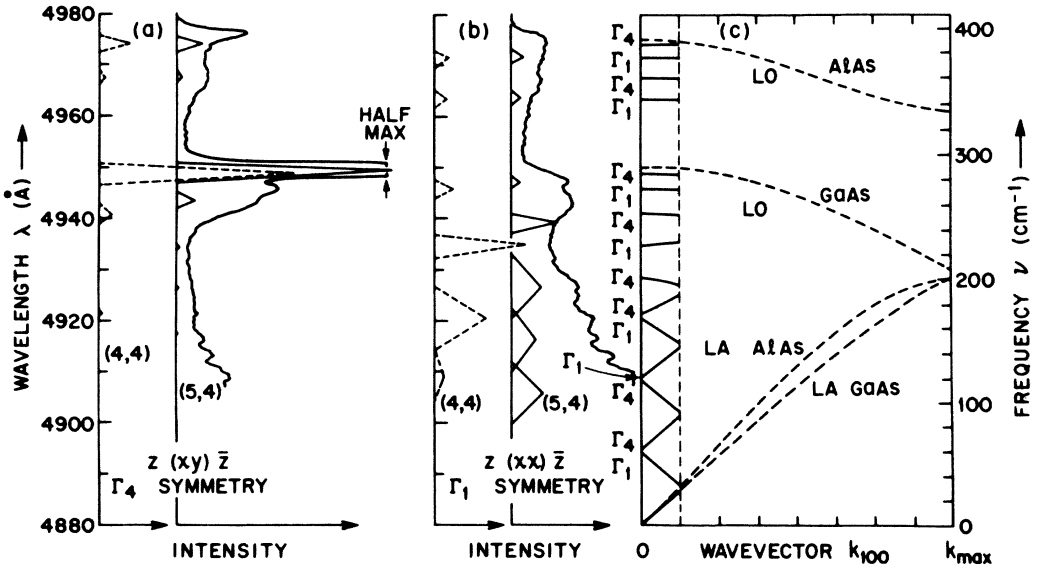

FIG. 7. Raman-scattering results for the tetralayer ($TT1$) sample, showing calculated and experimental spectra for (a) $z(xy)\bar{z}$ and (b) $z(xx)\bar{z}$ scattering geometries. Increasing wavelength (frequency) is plotted along the ordinate. The calculated spectra were obtained from the linear chain model using both a (4, 4) ordering of the layers (broken triangles) and (5, 4) ordering (solid triangles). Most of the calculated mode strengths are plotted assuming a linewidth of ~ 8 cm^{-1}; however, modes below 200 cm^{-1} in (xx) symmetry are plotted with assumed widths of ~ 35 cm^{-1} to more accurately fit the experimental data. Longitudinal modes in the full Brillouin zone of GaAs are plotted in (c) for both GaAs and AlAs, along with the reduced zone for a (4, 4) tetralayer sample.

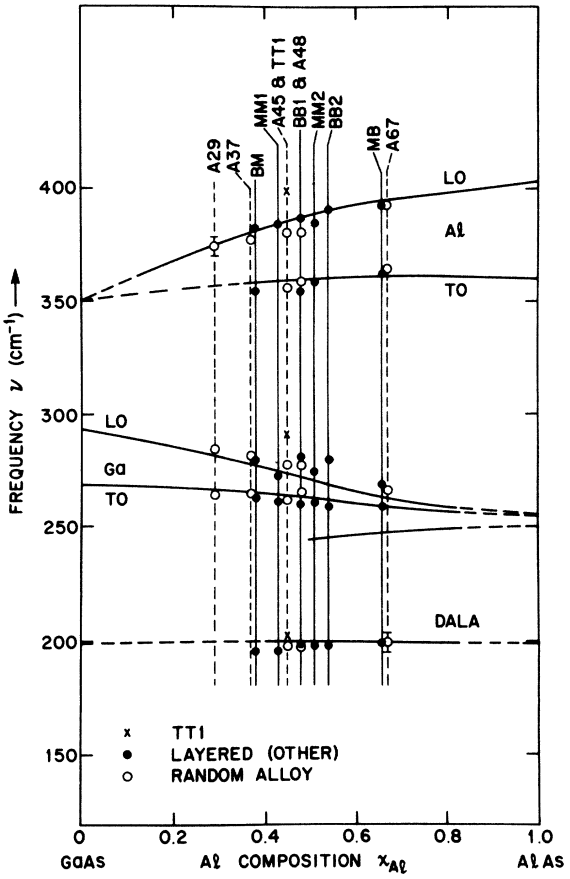

FIG. 8. Frequencies of principal phonons observed by Raman scattering as a function of average Al composition. Solid (and broken) curves are from the results of Tsu *et al.* (Ref. 20) for random alloys.

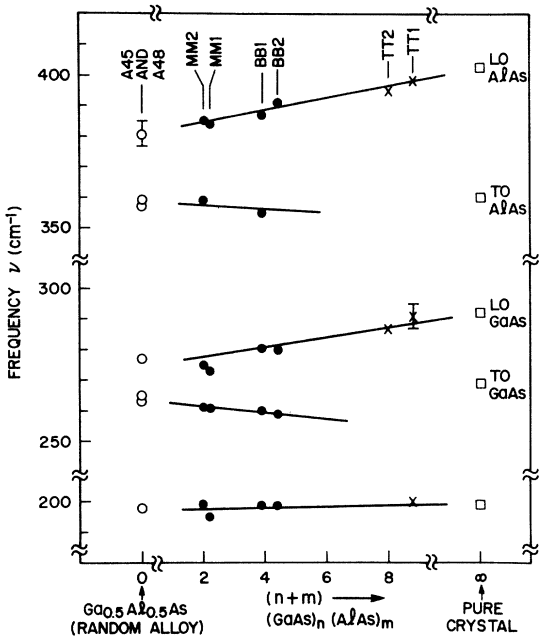

FIG. 9. Frequencies of principal phonons observed by Raman scattering for samples with nominal aluminum content of ~ 50 percent. The samples are plotted against the length of the new lattice period to illustrate the effects of layering.

C. Discussion

1. Energies of the principal phonons

The two dominant features of all the spectra reported here are the LO phonons corresponding to Al-As vibrations and Ga-As vibrations. The energies of these modes have been determined for all samples, and are plotted as a function of average Al composition in Fig. 8, along with the results obtained by Tsu *et al.*[20] for random alloy samples. In general, mode frequencies for both the layered samples and random alloys follow the same overall compositional dependence. In addition, however, there is a tendency for the energies of the LO modes of the layered samples to be slightly greater than those of the alloys, and for the LO-TO splittings to be greater. These results suggest replotting the principal mode frequencies as a function of a parameter which measures the layer ordering; this is done in Fig. 9. Now the effect of layering is evident; a clear trend is observed for phonon frequencies in the sequence of samples: *MM-BB-TT*. In the case of the *TT* samples, the energies of the LO vibrations of Al-As and Ga-As are identical (to within experimental error) to the LO phonons of pure AlAs and GaAs, respectively. The dominant scattering events of the *TT* sample therefore display the character of isolated regions of bulk AlAs and GaAs, a strong indication of order in the layer structure.

2. Fine-structure and zone-folding effects

Model calculations for layered structures predict additional (though often weak) modes in the optical spectra of these samples due to zone folding, as discussed above. This fine structure is observed in the spectra for the *TT* samples, Fig. 7, for which a multiplicity of lines is expected. Figure 7 includes a diagram showing the phonon dispersion curve calculated from the linear chain model. The full Brillouin zone (BZ) is shown, giving the longitudinal modes for GaAs and AlAs. For the *TT* case, the BZ is one-eighth the size of that for GaAs, since the layer period is eight molecular layers. The large number of new zone-center phonons in the reduced BZ is apparent.

The experimental spectra obtained from sample *TT*1 for both scattering geometries are shown in Figs. 7(a) and 7(b). Increasing wavelength is plotted along the ordinate for comparison with the phonon dispersion curves. Also shown are theo-

retical spectra calculated from the linear chain model for a (4,4) sample, indicating the Raman energies and strengths of all modes of both symmetries. (Linewidths have been adjusted to correspond roughly with experimental linewidths.) The agreement between theory and experiment is quite good. If, however, the calculation is modified to more closely approximate the actual (4.8,4) layer structure of this sample with a (5,4) linear chain, the theoretical fit to the data improves, and a close approximation to the experimental results is obtained. Note that the forbidden 201-cm^{-1} mode arising from the zone boundary need not be invoked, since the (5,4) sample has a strong, allowed mode at 196 cm^{-1}. New vibrational modes resulting from zone-folding effects have clearly been observed for this sample, and the linear-chain model can predict these modes with good accuracy.

3. *Disorder and the 201-cm^{-1} mode*

A mode near this frequency has been seen in all samples within the composition range $0.3 \leq x_{\mathrm{Al}}^{\mathrm{av}} \leq 0.7$, regardless of whether the sample is a random alloy or layered. As discussed in Sec. II B, the DALA mode in the random alloy is known to be a weak transition of the zone-boundary LA phonon, made possible by the lattice disorder. For layered samples with equal numbers of GaAs and AlAs layers ($n=m$), this phonon appears at the zone center. If n and m are odd, the 201-cm^{-1} mode should become quite strong. However, for even $n=m$, an exact cancellation of lattice polarizability occurs which gives the mode zero strength in Raman scattering, if nearest-neighbor forces alone are considered. These arguments suggest that the vibration at 201 cm^{-1} should be weakest in the random alloy (DALA), somewhat stronger in samples *BB* and *TT*, and strongest in *MM*. Experimentally, there is a tendency for the data to agree with this model, but the results are by no means unambiguous (Table VI). This imperfect agreement is believed to result from the lack of a perfectly sharp boundary between the GaAs and AlAs layers. Comparison of the data in Table VI with mode strengths calculated for disordered monolayers on the basis of cation interchange (Fig. 4) suggests that ~20% to 30% of the cations in the interface regions are on the wrong sites, since the 201-cm^{-1} mode is usually observed to be only a factor of 1 to 2 times stronger than the DALA band.

4. *Linewidths*

Large variations in the linewidths of the principal LO phonons were noted in these studies. Results are given in Table VII for the Ga-As and Al-As vibrations. The data recorded in this table are averages over several measurements (at least four runs, sometimes as many as 10), and are corrected for instrumental broadening ($\Gamma_{\mathrm{inst}} = 6.8$ cm^{-1}) using $\Gamma = (\Gamma^2_{\mathrm{observed}} - \Gamma^2_{\mathrm{inst}})^{1/2}$. The most noticeable trend in these data is the narrowing of the linewidth of the GaAs-like phonon when the sample composition is rich in Ga, and narrowing of the AlAs-like mode for high Al composition. This is particularly striking for the high Al case ($x_{\mathrm{Al}}^{\mathrm{av}} \simeq 0.67$), for which the GaAs-like phonon is two to three times the width of the AlAs-like mode. In most cases, the results seem to depend little on whether the sample is periodic or a random alloy, and most samples have considerably broader lines than good quality crystals of pure GaAs. However, a significant exception is the tetralayer sample *TT*, having the narrowest linewidths of all the ternaries studied in this work; the GaAs-like mode in sample *TT* has essentially the same width as pure GaAs. This result again demonstrates that the tetralayer sample is well ordered.

TABLE VII. Linewidths of principal LO phonons measured by Raman scattering. Errors quoted are standard deviations from averages of several measurements.

Sample	LO linewidth (cm^{-1}) GaAs-LO	AlAs-LO
BM	8.0 ± 0.3	9.4 ± 2.1
*A*29	6.8	10.0
*A*37	6.5	9.8
*MM*1	9.9 ± 1.1	8.3 ± 0.3
*MM*2	10.2 ± 0.8	9.4 ± 0.7
*BB*1	9.5 ± 0.4	8.7 ± 2.5
*BB*2	10.4 ± 0.3	8.0 ± 0.7
*TT*1	4.5 ± 0.6	3.7 ± 1.4
*A*45	9.2	8.5
*A*48	8.7	8.3
MB	14.9 ± 1.6	5.2 ± 0.4
*A*67	11.8 ± 1.0	5.1 ± 0.6
GaAs	4.0	···

VI. INFRARED ABSORPTION

A. Absorption spectra and transverse optical frequencies

Room-temperature transmission measurements have been made on layered samples over the frequency range 150–1000 cm^{-1}. Sample thicknesses were all in the range 3–4 μm. For these thicknesses the spectra show strong absorption at the principal transverse-optical phonon frequency as well as a pattern of fringes due to interference away from these frequencies. The fringes allow the accurate calculation of the product of thickness times index of refraction. Because of an un-

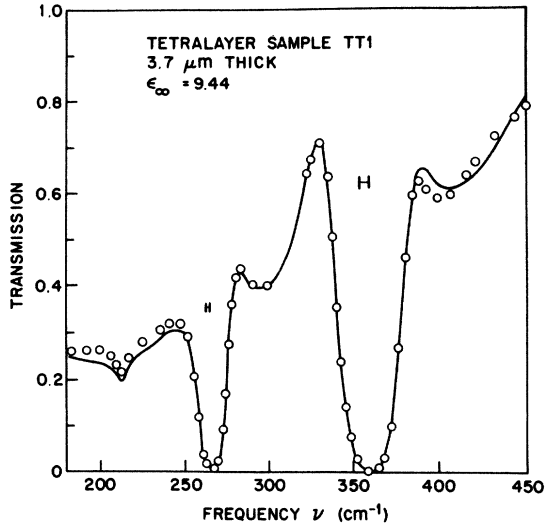

FIG. 10. Infrared transmission spectrum for sample *TT*1 at room temperature. Experimental data are shown as open circles. The solid curve is the best fit obtained by using classical oscillators as described in the text. The bars show the resolution of the spectrometer near each mode. Resolution effects have been included by smearing the fitted curve according to the resolution of the spectrometer.

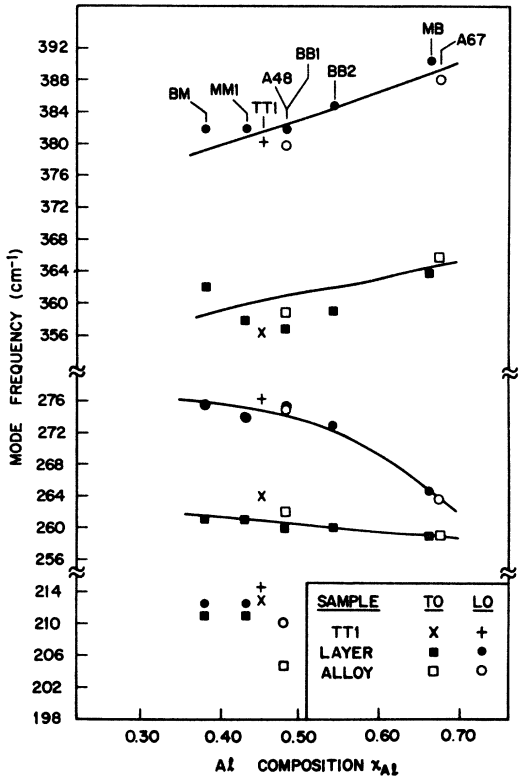

FIG. 11. Mode frequencies for six layered samples and two alloy samples from transmission spectrum analysis. The samples are displaced horizontally according to their nominal atomic fraction of Al.

certainty in thickness of ±10% there is a corresponding uncertainty in the high-frequency dielectric constant ϵ_∞. Figure 10 shows a typical spectrum. The principal TO phonons are readily identified near 260 and 360 cm^{-1}, and a weak absorption can be seen near 213 cm^{-1}. The remaining two dips are interference fringes. The fits to be described below show that for typical samples such as *TT*1 the TO frequency is 3 to 5 cm^{-1} lower than the center of the strong absorption feature in the spectrum.

Fits to the transmission were carried out using sums of the classical oscillator absorption terms to represent the absorption peaks in the spectra.[33] The high-frequency dielectric constant ϵ_∞ was chosen by assuming a linear variation between the values for pure AlAs and GaAs and using the average composition (percentage Al in the sample) regardless of whether the structure is layered or not. We use $\epsilon_\infty(\text{GaAs}) = 11.1, \epsilon_\infty(\text{AlAs}) = 8.2$. This procedure yields fringes at the correct frequencies to within the uncertainty mentioned above for sample thickness. The solid curve in Fig. 10 shows the best fit for the *TT* sample. In the fitting routine five oscillator modes were introduced, one for the mode near 360 cm^{-1}, three for the mode near 260 cm^{-1} since it is quite asymmetric, and one for the weak mode at 213 cm^{-1}. The finite resolution of the spectrometer is allowed for by broadening the calculated spectra using a method similar to that described by Berreman.[34] Similar fits were carried out for seven other samples. The fitted TO frequencies are shown in Fig. 11. These frequencies have an absolute precision of better than ±1 cm^{-1}.

B. Longitudinal-optical mode frequencies

In the process of fitting the absorption as described above, an accurate measure of the strength of each principal phonon is obtained. These strengths together with the value of ϵ_∞ can be used to find the zeros in the dielectric constant and thus obtain the LO mode frequencies. The circles and + in Fig. 11 show the LO frequencies obtained by this technique. For one sample, a separate reflection measurement was made of the two principal reststrahlen bands near 260 and 360 cm^{-1}. A separate set of fits to this reflectivity allowed an independent determination of the TO and LO frequencies for this sample. These frequencies agreed within ±1 cm^{-1} with the ones obtained by the transmission analysis described in Sec. VI A. Figure 12 shows the TO and LO mode structure for the sample of Fig. 10. The asymmetry of the mode near 260 cm^{-1} is readily apparent.

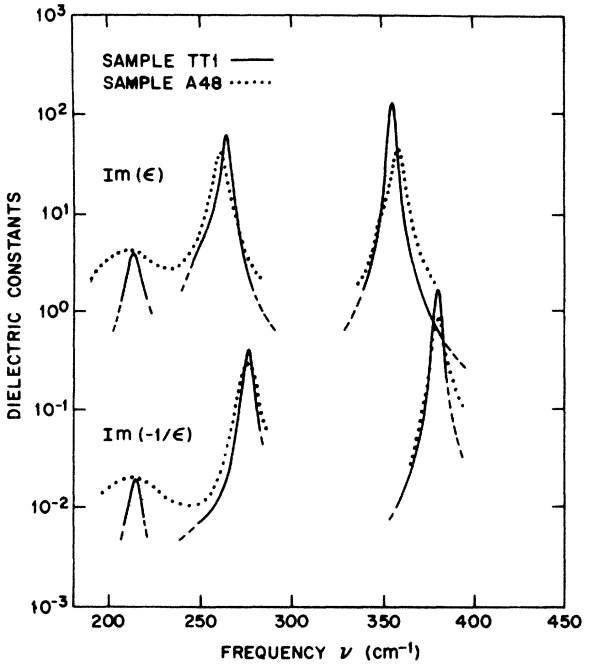

FIG. 12. Transverse-optical mode spectrum $\mathrm{Im}(\epsilon)$ and longitudinal-optical mode spectrum $\mathrm{Im}(-1/\epsilon)$ for sample $TT1$ and $A48$. These dielectric functions are obtained from the transmission data analysis and therefore refer to polarization along the x (or y) crystalline direction. The ratio of peak strengths near 213 cm^{-1} suggests ~25% disorder in $TT1$ compared with complete disorder of $A48$.

C. Discussion

All samples showed two main TO modes and two main LO modes (see Fig. 12) whose frequency depends on the exact nature of the sample. Figure 11 shows evidence for layering in sample $TT1$. Note that Table II shows that the gaps that form in the (4,4) model cause the GaAs-like vibration to be only 1.1 cm^{-1} below the mode of pure GaAs. Our data for the samples other than the $TT1$ sample in the composition range 0.4 to 0.5 all exhibit a TO frequency much lower, near 261 cm^{-1}. The significantly higher frequency of 264 cm^{-1} for TT suggests that the principal strength in this band arises from vibrations of groups of GaAs in unison implying the presence of layers. The TO modes in the Al-like branch near 360 cm^{-1} do not give a similarly clear picture. There is considerable scatter in the frequencies though each point has a precision of ±1 cm^{-1}. This behavior is not understood though it may be related to the very different eigenvectors in the Ga-like and Al-like branches. The large amplitude on every Al ion in the Al-like branch near 360 cm^{-1} suggests that any disorder more strongly perturbs frequencies in this branch than in the Ga-like branch.

All of the samples exhibited a similar asymmetric shape for the mode near 260 cm^{-1}. Table II shows that a zone-folded mode is expected about 6 cm^{-1} below the main mode in a (4,4) sample. No such mode is expected however for the (1,1) and (2,2) samples. We therefore associate the mode broadening on the low frequency side with some degree of randomness in all of these samples since the same broadening is found in the alloy samples and all calculations with disordered linear chains give weak bands of modes on the low-frequency side of the strongest TO mode.

Four samples show modes near 212 cm^{-1} (Figs. 10–12). The absorption near the peak of these modes is $\alpha_{\max} \sim 1300$ cm^{-1}. Studies of pure GaAs show an absorption minimum with values of α near 20 to 30 cm^{-1} at this frequency.[35] These modes therefore represent a very significant absorption process. From Table II and Fig. 3 we note that while there is a phonon branch folded to the zone center near this frequency it is not infrared active. Under the assumptions used in constructing the model, the branch near 200 cm^{-1} is purely longitudinal. In the real crystal, however, an Al(Ga) ion which diffused into or grows in a plane which is predominantly Ga(Al) perturbs the vibration pattern. We believe the infrared modes are associated with such disorder. We cannot properly calculate such three-dimensional disordering and its effect on infrared absorption using the chain model. Note that the one-dimensional disorder calculations (Fig. 4) are valid for the longitudinal branches and induced longitudinal modes but not for induced transverse modes. We find, however, that calculations using chain models disordered in various ways do create modes with longitudinal dipole moment in the range 170 to 201 cm^{-1} and modes with Raman activity in the same range. The activated Raman modes show a tendency to lie at lower frequencies. We conclude that the infrared modes near 212 and some of the Raman modes near 200 cm^{-1} arise from disorder activation of the LA branch.

The random alloy sample $A48$ shows a mode near 200 cm^{-1} four times greater in integrated strength than the 212-cm^{-1} mode in $TT1$ (Fig. 12). By direct but simplified analysis this result suggests that either the $TT1$ sample has a random pattern of 25% of the sites with wrong ion occupancy or that 75% of the sample is perfectly layered and 25% is disordered. The Raman-mode frequencies and linewidths and the infrared-mode frequencies strongly suggest the former interpretation. Some samples shown in Fig. 11 had too small an area for good signal to noise below 250 cm^{-1}. Thus the presence or absence of a 212-

cm^{-1} mode was not established.

When the strong modes shown in Fig. 11 are compared with the modes determined by Raman scattering we find general agreement on the TO mode frequencies in cases where the Raman spectra showed this mode. The LO frequencies are significantly different however. If we consider the group of four samples whose nominal composition ranges from 43% to 51% Al we find that both the AlAs LO mode and the GaAs LO mode range from 2 to 6 cm^{-1} lower in the infrared spectrum but the TT sample lies 14 to 16 cm^{-1} lower. This is a true anisotropy effect in the crystals since the infrared spectrum gives data on the LO mode polarized along x and the Raman spectrum, the mode polarized along z. An independent check was made on a separate sample $TT2$ grown for this purpose. Using carefully calibrated spectrometers the result was the same. The LO mode polarized along x lay 13 cm^{-1} below the frequency of the LO mode polarized along z. A portion of this difference appears to be connected with strain since it occurs in alloy samples which have no long-range layering effects. The large effect in the tetralayered sample indicates however that there is some phonon anisotropy associated with layering.

VII. CONCLUSIONS

(a) The linear-chain model with nearest-neighbor forces can be used to give a reasonable approximation to the phonon frequencies and strengths in pure and layered samples. Deviations from perfect ordering of the layers can be included in this model by substitution of selected cation masses. Fits to the spectra establish values for the relative Raman polarization of GaAs and AlAs and for the diagonal polarizability which is normally unmeasurable.

(b) Direct evidence of well-ordered layer growth by MBE has been obtained for a sequence of alternating tetralayers: four molecular layers of GaAs, followed by four molecular layers of AlAs. The evidence for this from the Raman scattering experiments is threefold: (i) the energies and (ii) the linewidths of the principal GaAs-like and AlAs-like phonons correspond to those observed in the pure crystals, and (iii) the large multiplicity of fine structure anticipated from the model as a result of zone-folding effects has been observed in both (xx) and (xy) scattering. In addition, the main features seen in the infrared spectra also show the tetralayer modes with significant shifts away from the modes of nearly all other samples. The 213-cm^{-1} infrared mode when compared with the absorption in pure GaAs and in the alloy $Ga_{0.52}Al_{0.48}As$ shows that there is a new periodicity quite distinct from a random arrangement of cations, although there is also some disorder.

(c) For alternating mono- and bilayers, there is some indication of layer effects; in particular, the 201-cm^{-1} mode is very strong in $MM1$ and generally weak in BB and TT samples. A weaker mode at this same frequency appears in alloy samples and is identified as a DALA mode. DALA intensity may be present to some extent in all samples, however, so precise mode assignment is not possible. A comparison of $MM1$ with other samples and with Fig. 4 suggests that the occupancy factor of Ga(Al) on the Ga(Al) sublattice is not 1.0 but between 0.7 and 0.8 (x in Fig. 4 between 0.2 and 0.3; note that $x = 0.5$ means a random arrangement). Because of the layering effects seen in our $TT1$ sample and seen by other techniques[26,36] in samples with longer periodicities we form the following picture of the layering arrangement. Next to a GaAs-AlAs interface the first cation plane has a 20 to 30 percent probability of containing the wrong cation. These wrong cations are probably not randomly scattered over the entire plane but may all lie in a contiguous area as a result of a growth step. The fact that (4,4) and thicker layers show ordered growth implies that the layers containing disordered cations rarely extend more than one atom from the interface. Such regions have a fractionally larger effect on (1,1) and (2,2) samples than on (4,4) or $m,n > 4$ samples.

ACKNOWLEDGMENTS

The authors gratefully acknowledge the important contributions of W. Wiegmann in growing the crystals used in this study, and J. A. Ditzenberger and A. M. Sergent in mounting samples and making spectral measurements; L. Kopf and R. Dingle gave assistance with sample etching and composition evaluation. Finally, several helpful conversations were held with M. A. Schlüter and R. Loudon.

[1] A. Y. Cho and J. R. Arthur, Prog. Solid State Chem. 10, 157 (1975).

[2] L. L. Chang, L. Esaki, W. E. Howard, and R. Ludeke, J. Vac. Sci. Technol. 10, 11 (1973).

[3] R. Dingle, W. Wiegmann, and C. H. Henry, Phys. Rev. Lett. 33, 827 (1974).

[4] R. Dingle, A. C. Gossard, and W. Wiegmann, Phys. Rev. Lett. 34, 1327 (1975).

[5]A. C. Gossard, P. M. Petroff, W. Wiegmann, R. Dingle, and A. Savage, Appl. Phys. Lett. 29, 323 (1976).
[6]A preliminary account of Raman-scattering results on layered and disordered samples has been given by J. L. Merz, A. S. Barker, Jr., and A. C. Gossard, Appl. Phys. Lett. 31, (15 July 1977).
[7]G. C. Trigunayat and A. R. Verma, in *Crystallography and Crystal Chemistry of Materials with Layered Structures* (Reidel, Dordrecht, Holland, 1976), p. 269.
[8]D. W. Feldman, J. H. Parker, Jr., W. J. Choyke, and L. Patrick, Phys. Rev. 173, 787 (1968).
[9]A. Polian, K. Kunc, and A. Kuhn, Solid State Commun. 19, 1079 (1976).
[10]C. Kittel, *Introduction to Solid State Physics*, 3rd ed. (Wiley, New York, 1968), Chap. 5.
[11]J. L. Yarnell, J.L. Warren, R. G. Wenzel, and P. J. Dean, in *Neutron Inelastic Scattering* (IAEA, Vienna, 1968), Vol. 1, p. 301.
[12]G. Dolling and J. L. T. Waugh, in *Lattice Dynamics*, edited by F. R. Wallis (Pergamon, Oxford, 1965), p. 19.
[13]M. Ilegems and G. L. Pearson, Phys. Rev. B 1, 1576 (1970).
[14]A. Onton and R. J. Chicotka, Phys. Rev. B 10, 591 (1974).
[15]It is known from optical experiments that both zone-center and X-point phonon frequencies decrease when GaAs is mixed with AlAs. The decrease is about 5% to 10% (depending on the particular phonon) for a 50:50 crystal independent of whether that crystal is an alloy or is layered. The model therefore should give approximately the correct frequency for the important LA X-point phonon in the layered crystal.
[16]Test calculations for longitudinal modes and comparisons with the frequencies of GaAs (Ref. 12) and our own results for crystal $TT1$ suggest that Ga-Ga and As-As second-neighbor forces are about 10% of the nearest-neighbor forces but that Al-Al forces are much smaller.
[17]A. S. Barker, Jr., Phys. Rev. 136, A1290 (1964).
[18]R. Tsu and S. S. Jha, Appl. Phys. Lett. 20, 16 (1972).
[19]A. S. Barker, Jr. and R. Loudon, Rev. Mod. Phys. 44, 18 (1972).
[20]R. Tsu, H. Kawamura, and L. Esaki, in *Proceedings of the International Conference on the Physics of Semiconductors, Warsaw, 1972* (Elsevier, Amsterdam, 1972), Vol. 2, p. 1135.
[21]A. S. Barker, Jr. and A. J. Sievers, Rev. Mod. Phys. Suppl. 47, S1 (1975).
[22]*International Tables for X-Ray Crystallography, Vol. I, Symmetry Groups*, edited by N. F. M. Henry and K. Lonsdale (Kynoch, Birmingham, England, 1952).
[23]We follow the customary designation for Raman scattering, describing the scattering geometry as $k(ij)k'$, where k and k' refer to the incident and scattered wave-vector directions, respectively, and i and j refer to their respective polarizations. Since $k=z$ and $k'=\bar{z}$ in this study the notation will be abbreviated to (ij) for the remainder of the paper.
[24]R. Loudon, Adv. Phys. 13, 423 (1964).
[25]G. F. Koster, J. O. Dimmock, R. G. Wheeler, and H. Statz, *Properties of the Thirty-Two Point Groups* (MIT, Cambridge, Mass., 1963).
[26]P. D. Dernier, D. E. Moncton, D. B. McWhan, A. C. Gossard, and W. Wiegmann, Bull. Am. Phys. Soc. 22, 293 (1977).
[27]M. D. Sturge, Phys. Rev. 127, 768 (1962).
[28]D. D. Sell and H. C. Casey, Jr., J. Appl. Phys. 45, 800 (1974).
[29]H. C. Casey, Jr., D. D. Sell, and K. W. Wecht, J. Appl. Phys. 46, 250 (1975).
[30]M. A. Afromowitz (unpublished).
[31]M. A. Afromowitz, J. Appl. Phys. 44, 1292 (1973).
[32]Ditric Optics 3 cavity filter with 70-Å bandwidth, used at varying angles of incidence ($0\leq\theta_i\leq 10°$) to tune filter.
[33]H. W. Verleur, J. Opt. Soc. Am. 58, 1356 (1968).
[34]D. W. Berreman, Appl. Opt. 7, 1447 (1968).
[35]R. H. Stolen, Appl. Phys. Lett. 15, 74 (1969).
[36]P. M. Petroff, A. C. Gossard, W. Wiegmann, and A. Savage, Bull. Am. Phys. Soc. 22, 293 (1977); J. Cryst. Growth (to be published).